Exchange interactions in the quasi-one-dimensional mixed antiferromagnet $CsCo_{1-x}Fe_xCl_3$: A light-scattering study

R. W. G. Syme* and D. J. Lockwood
Division of Microstructural Sciences, National Research Council, Ottawa K1A 0R6, Canada
(Received 21 March 1985)

The polarized Raman spectra of $CsCo_{1-x}Fe_xCl_3$ crystals have been measured at 4 K over the range 20–1400 cm^{-1} for $x=0.02$ and 0.06. Spectral features arising from first-order scattering from Fe^{2+} electronic excitations have been identified and the effective Co^{2+}-Fe^{2+} exchange interaction determined from a crystal-field fit to energy levels of the $^5T_{2g}$ (^5D) term of an Fe^{2+} ion in a trigonal site with spin-orbit and exchange interactions. This exchange interaction has, in turn, been used to identify additional features in the spectra associated with broken-chain Co^{2+} electronic excitations and with double excitation of Co^{2+}-Fe^{2+} pairs. Scattering by the Co^{2+} full-chain magnon and 300-cm^{-1} exciton has been studied over the temperature range 3–40 K and is discussed in relation to the competing one-dimensional magnetic alignments in $CsCoCl_3$ (antiferromagnetic Ising) and $CsFeCl_3$ (ferromagnetic X-Y). The effect of x on electron-phonon coupling for the E_{1g} phonon is also discussed.

I. INTRODUCTION

Cesium trichlorocobaltate ($CsCoCl_3$) and cesium trichloroferrate ($CsFeCl_3$) are both known to exhibit pronounced one-dimensional (1D) magnetic behavior at low temperature.[1–9] At sufficiently low temperatures $CsCoCl_3$ orders three dimensionally and is a fully ordered ferrimagnet for $T<T_N^{II}=8.5$ K and a partially ordered antiferromagnet for $T<T_N^{I}=20.8$ K.[4,5] On the other hand, $CsFeCl_3$, which has a singlet ground state, exhibits no long-range magnetic order for temperatures as low as 0.8 K, except in the presence of an applied magnetic field $B>3.8$ T.[7,9] These crystals are isomorphic[10–12] to $CsNiCl_3$, which has a hexagonal structure[13] (space group $P6_3/mmc$ with $Z=2$) comprising linear chains of face-sharing $NiCl_6^{4-}$ octahedra lying along the c axis, these chains being separated by the large Cs^+ ions. Distortion of the octahedra gives a trigonal site symmetry (D_{3d}) for each Ni^{2+} ion. For both $CsCoCl_3$ and $CsFeCl_3$ the exchange interaction between the divalent transition-metal ions along the c-axis chain is much larger than the interchain exchange, giving rise to the 1D magnetic behavior. There is, however, an important contrast between the two compounds, in that for $CsCoCl_3$ the preferred spin alignment is along the c axis, giving a 1D Ising-like antiferromagnet,[1,2] while for $CsFeCl_3$ the intrachain interaction is ferromagnetic with the preferred spin alignment perpendicular to the chain axis.[6–8] Previous work on mixed crystals of this type has been confined to the $CsCo_{1-x}Mg_xCl_3$ system,[14–17] in which the cobalt chains are diluted by substitution of diamagnetic Mg^{2+} ions. Features of the Raman scattering arising from single Co^{2+} ions, Co^{2+}-Co^{2+} pairs, and broken-chain Co^{2+} ions were identified[15] in addition to the magnon, exciton (full-chain Co^{2+}), and phonon structure of pure $CsCoCl_3$. The spin-wave response has also been determined by inelastic neutron scattering.[17] An unusual concentration dependence of the E_{1g}-phonon scattering [at 118 cm^{-1} in pure $CsCoCl_3$ (Ref. 3)] has been noted.[14] Short- and long-range magnetic ordering of this magnetically dilute system has been investigated using linear birefringence and NMR techniques.[16]

We report here the first study of dilution of the cobalt chains in $CsCoCl_3$ with another paramagnetic ion (in this case, up to 6 at. % Fe^{2+}). This work forms part of a systematic study of the effect of various transition-metal dopants (M) in $CsCoCl_3$, using Raman scattering as a probe of both the magnetic structure and the low-energy electronic excitations of each $CsCo_{1-x}M_xCl_3$ system. The appropriate intrachain exchange interaction may be obtained from a crystal-field analysis of the observed electronic structure. In addition, study of the temperature dependence of magnon and exciton scattering gives information concerning the interchain exchange and certain aspects of electron-phonon coupling in these systems.

The format of the paper is as follows. The experimental method and results are described in Secs. II and III, followed by a detailed analysis and discussion of the various aspects of this study in Sec. IV and a concluding summary of the results in Sec. V.

II. EXPERIMENT

Boules of $CsCo_{1-x}Fe_xCl_3$ typically 10 mm in diameter and 50 mm long were grown from the melt in quartz ampoules using the Bridgman-Stockbarger method. Samples were prepared by cleaving the boules under a dry nitrogen atmosphere and were mounted in a Thor S500 continuous-flow cryostat, where the sample is cooled by conduction and helium exchange gas. The crystal c axis (or Z direction) was identified from the intersection of $\{11\bar{2}0\}$ cleavage planes. The cleaved surfaces were of good optical quality and required no further polishing.

Raman scattering measurements were carried out in the 90° scattering geometry, $X(--)Y$, with the Y direction

chosen normal to a $[11\bar{2}0]$ cleavage plane and with the incident laser beam close to the crystal surface to maximize the Raman signal. The spectra were excited with 100 mW of filtered argon-laser radiation at 476.5 or 496.5 nm. The 496.5-nm laser line gave a stronger signal for the Fe^{2+} electronic scattering than the 476.5-nm line used by Johnstone *et al.*[14,15] in their study of $CsMg_{1-x}Co_xCl_3$. The surface temperature of the crystal was monitored using a gold-iron—Chromel thermocouple and laser heating of the sample was estimated to be less than 2 K. The scattered light was analyzed using a Polaroid filter, dispersed with a Spex 14018 double monochromator at a spectral resolution of 2.9 cm^{-1} at 476.5 nm (2.7 cm^{-1} at 496.5 nm) and detected with a cooled RCA 31034A photomultiplier, all spectra being recorded under computer control.[18]

The actual samples used in the two experiments were analyzed for cobalt and iron content by inductively-coupled-plasma atomic-emission spectroscopy and found to have x values of 0.0174 ± 0.0008 and 0.061 ± 0.001. Small concentration gradients were evident within the boules, and for the purpose of discussion these crystals will be referred to as $x=0.02$ and 0.06, respectively. Trace amounts of manganese (about 0.2 at. %) and nickel (about 0.1 at. %) were also detected in both samples, but we believe these other impurity levels to be too low in comparison to the iron to have given rise to any of the observed spectral features.

III. RESULTS

The polarized Raman spectra of $CsCo_{1-x}Fe_xCl_3$ at 4 K, for $x=0.02$ and 0.06 and for shifts of up to 1400 cm^{-1}, are presented in Figs. 1—3. For comparison, the spectrum of $CsCoCl_3$ recordered under similar conditions is also given in these figures. The pattern of $CsCoCl_3$ phonon scattering [56 cm^{-1} (E^a_{2g}), 138 cm^{-1} (E^b_{2g}), 189 cm^{-1} (E^c_{2g}), and 265 cm^{-1} (A_{1g}); cf. Ref. 14] is clearly repeated in the Fe-doped crystals with only minor frequency shifts. The magnon and coupled magnon-phonon (E_{1g}) scattering in the (70—125)-cm^{-1} region of the $X(ZX)Y$ spectrum is also evident for $x=0.02$ and, to a lesser extent, $x=0.06$, indicating that these levels of Fe doping may modify, but do not completely destroy, the magnetic ordering of the Co^{2+} ions at 4 K. There is evident, however, a considerable modification of other features of the spectrum, particularly in $X(ZZ)Y$ polarization, with much extra scattering throughout the energy range studied, including prominent new peaks at 48.5, 61.0, 225.0, and 274.5 cm^{-1}. In Sec. IV we interpret these extra features as electronic scattering from Fe^{2+} ions in the presence of an exchange field or from Co^{2+} ions perturbed by adjacent Fe^{2+} ions. That the extra scattering is electronic rather than vibrational in origin is supported by the observed temperature dependence of the scattering. The 4-K and 50-K $X(ZZ)Y$ spectra for $x=0.02$ are compared in Fig. 4, where it is seen that at 50 K the extra scattering is weaker than at 4 K compared to the intensity of the A_{1g} phonon, in line with the intensity variation of the Co^{2+} electronic scattering. Furthermore, none of the new features correlate with the reported Raman-active phonon frequencies[19] for $CsFeCl_3$. Apart from the E_{1g} phonon [at 143.5 cm^{-1} in $CsFeCl_3$ (Ref. 19) compared to 118 cm^{-1} in $CsCoCl_3$ (Ref. 3)], the $CsFeCl_3$ Raman-active phonons are about 5 cm^{-1} lower in frequency than the corresponding $CsCoCl_3$ phonons.

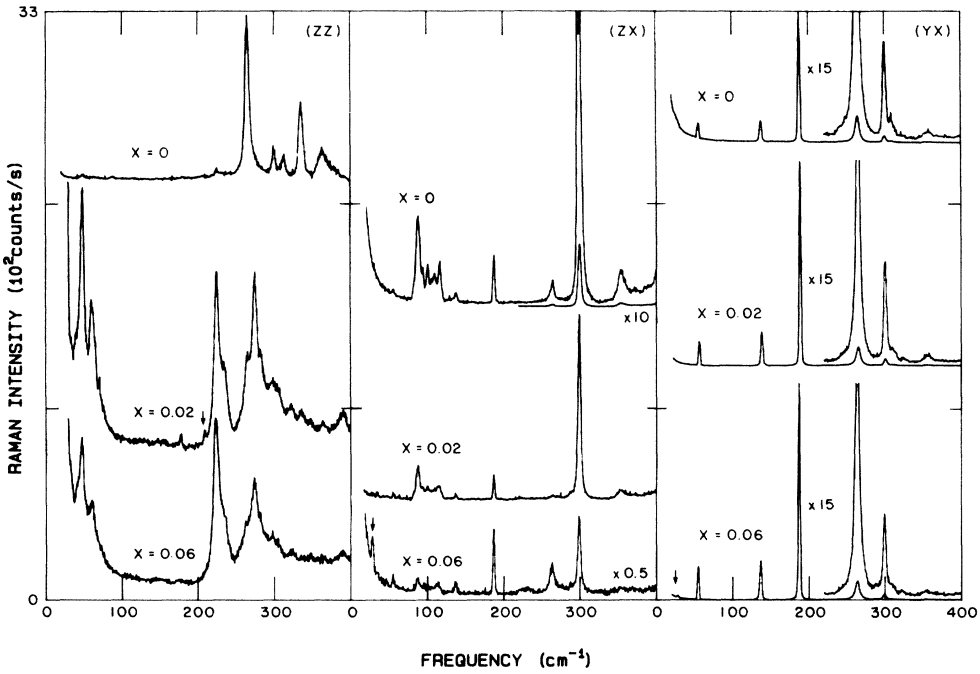

FIG. 1. Low-frequency Raman spectrum of $CsCo_{1-x}Fe_xCl_3$ measured at 4 K using 476.5-nm exciting light for $x=0$ and 0.02 [$X(YX)Y$ polarization], and 496.5 nm for $x=0.02$ [$X(ZZ)Y$ and $X(ZX)Y$ polarizations] and 0.06. The arrows mark laser-plasma-emission lines. Note the scale changes used for some spectra.

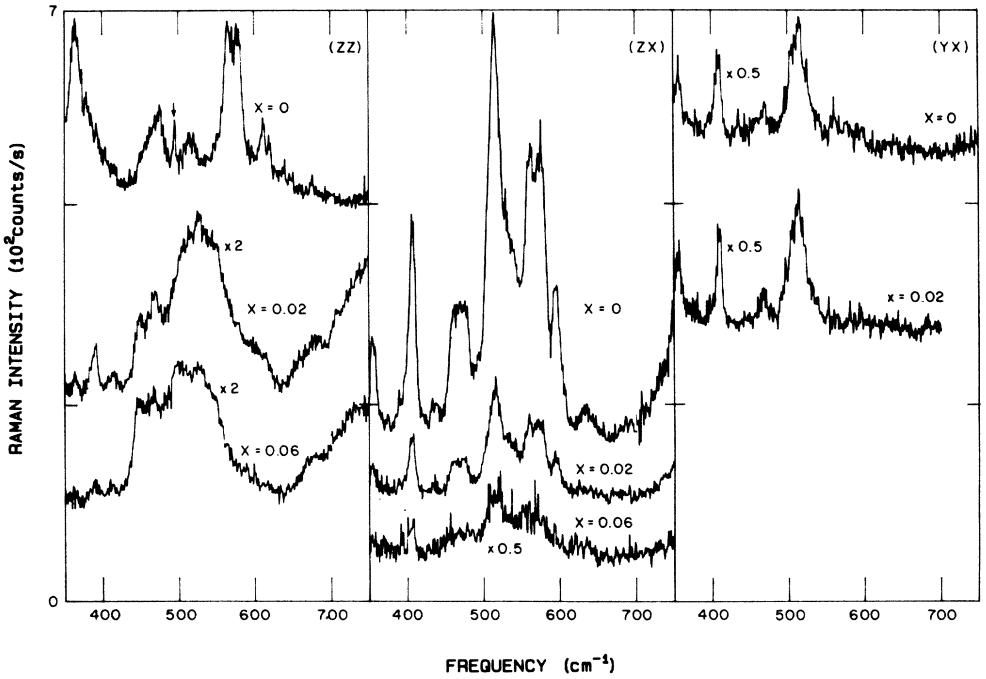

FIG. 2. Intermediate-frequency Raman spectrum of $CsCo_{1-x}Fe_xCl_3$ measured at 4 K for $x=0.02$ and 0.06, and at 10 K for $x=0$. The laser lines used were 476.5 nm for $x=0$ and 0.02 [$X(YX)Y$ polarization], and 496.5 nm for the other spectra. The arrow marks a laser-plasma-emission line. Note the scale changes used for some spectra.

The temperature dependence of the $X(ZX)Y$ scattering in the (70—130)-cm^{-1} region of the $CsCoCl_3$ magnon and E_{1g}-phonon scattering is shown in Fig. 5 over the ranges 3—40 K for $x=0.02$ and 3—20 K for $x=0.06$. A decrease in the $CsCoCl_3$ three-dimensional magnetic phase-transition temperatures with increase in Fe^{2+} concentration is evident. The Co^{2+} full-chain exciton near 300 cm^{-1} was also studied in detail over the range 3—25 K

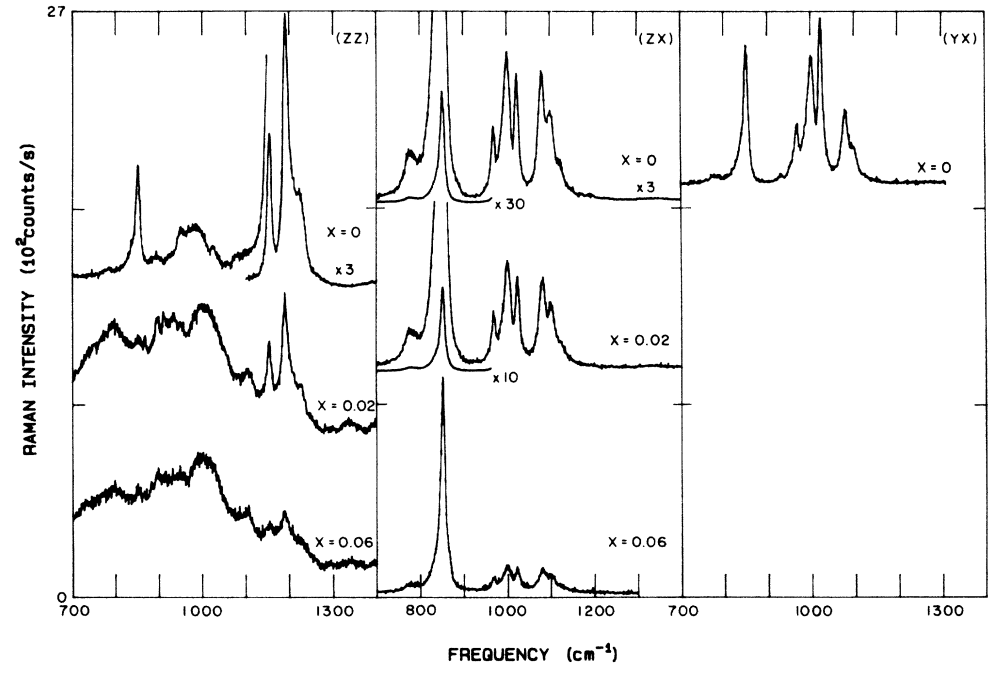

FIG. 3. High-frequency Raman spectrum of $CsCo_{1-x}Fe_xCl_3$ measured at 4 K for $x=0.02$ and 0.06, and at 10 K for $x=0$. The laser lines used were 476.5 nm for $x=0$ and 496.5 nm for $x=0.02$ and 0.06. Note the scale changes used for some spectra.

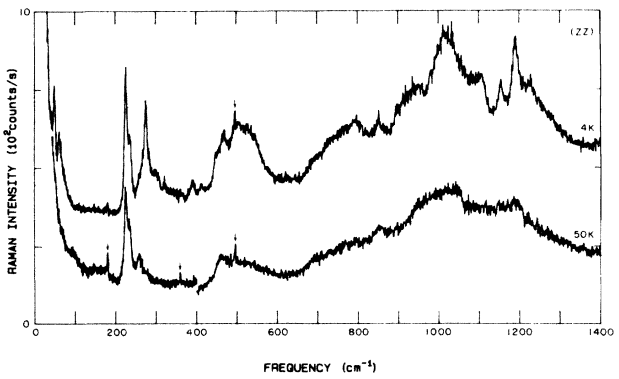

FIG. 4. Temperature dependence of the Raman spectrum of $CsCo_{0.98}Fe_{0.02}Cl_3$ recorded in $X(ZZ)Y$ polarization using a laser wavelength of 476.5 nm. The arrows mark laser-plasma-emission lines.

for the $x=0.02$ crystal, and some results are presented in Fig. 6. The variations with temperature in the frequency, linewidth, and integrated intensity of this feature are presented in Fig. 7. Within the experimental uncertainty the integrated intensity of the weak shoulder appearing in the high-energy wing of this exciton scattering in $X(YX)Y$ polarization was independent of temperature over the range studied. A similar weak feature is seen in $CsCoCl_3$ in this polarization. The 300-cm^{-1} exciton in the $x=0.06$ crystal decreased rapidly in intensity with increasing temperature over the range 4–20 K.

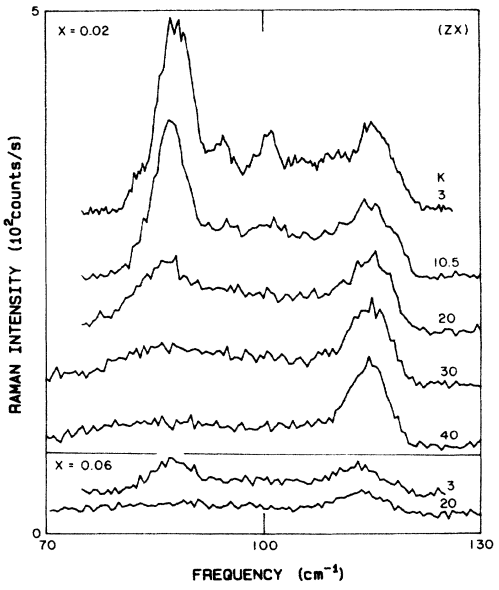

FIG. 5. Temperature dependence of the Co^{2+}-ion magnon feature in the Raman spectrum of $CsCo_{1-x}Fe_xCl_3$ recorded in $X(ZX)Y$ polarization using a laser wavelength of 496.5 nm.

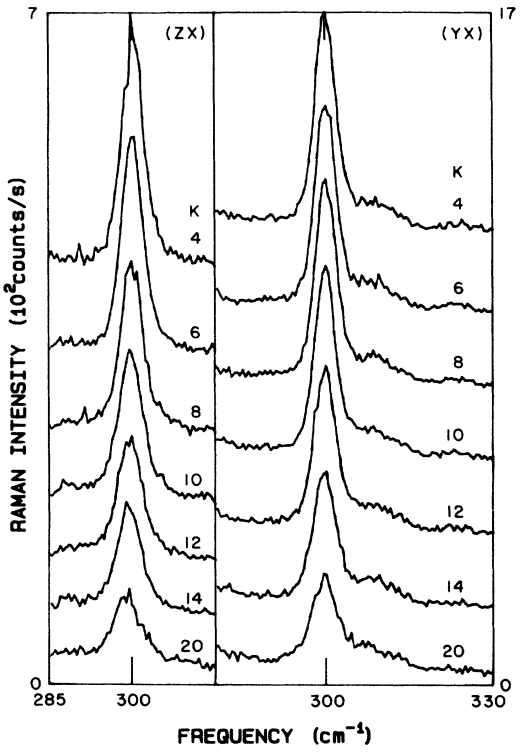

FIG. 6. Temperature and polarization dependences of the Co^{2+}-ion exciton feature near 300 cm^{-1} in the Raman spectrum of $CsCo_{0.98}Fe_{0.02}Cl_3$ recorded using a laser wavelength of 476.5 nm.

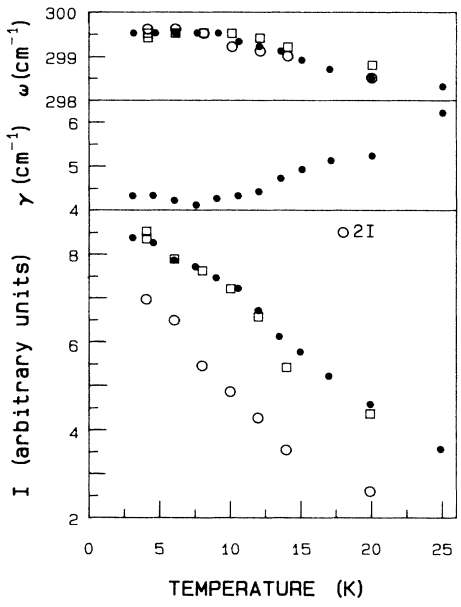

FIG. 7. Temperature dependences of the peak frequency (ω), full width at half maximum (γ), and integrated intensity (I) of the Co^{2+}-ion exciton near 300 cm^{-1}. The data were obtained from spectra recorded in $X(ZX)Y$ polarization using laser wavelengths of 496.5 nm (●) and 476.5 nm (○), and in $X(YX)Y$ polarization using a laser wavelength of 476.5 nm (□).

IV. DISCUSSION

A. Temperature and concentration dependences of Co^{2+} magnon and 300-cm^{-1} exciton scattering

The magnon spectra of Fig. 5 give some information on the effects of the added Fe^{2+} ions on the magnetic properties of $CsCoCl_3$. The 3-K spectrum for $x=0.02$ is similar to the 10-K spectrum of pure $CsCoCl_3$,[3] while the 3-K $x=0.06$ spectrum compares with the 20-K $x=0$ spectrum. Even allowing for the possibility that the laser heating in the iron-doped samples could be a little higher than that estimated in Sec. II, this comparison suggests that the doping produces an effect analogous to what occurs upon raising the temperature in pure $CsCoCl_3$, i.e., the Fe^{2+} ions disrupt the weak Co^{2+}-Co^{2+} nearest-neighbor interchain coupling but do not greatly affect the intrachain coupling for $x \lesssim 0.06$. This is probably because of geometrical effects. Only short chains, comprising three or more Co^{2+} ions, are needed to produce the observed magnon frequency in the 1D phase of $CsCoCl_3$,[15] whereas even for $x=0.02$ one in four chains of three Co^{2+} ions will have at least one Fe^{2+} ion as an interchain nearest neighbor.

The temperature dependences of the Co^{2+} full-chain magnon and 300-cm^{-1} exciton scattering have been used previously[20,21] to obtain information about the 3D magnetic ordering in $ACoX_3$ compounds (A denotes Cs,Rb; X denotes Cl,Br). In particular, the lowest exciton near 300 cm^{-1} in $CsCoBr_3$ and $RbCoCl_3$ exhibits a spin-dependent scattering mechanism involving interchain pairs of Co^{2+} ions.[21,22] The scattering intensity is thus a measure of the 3D ordering, and a distinct point of inflection in the intensity-versus-temperature behavior occurs at T_N^{I}. In an attempt to determine T_N^{I} in $CsCo_{0.98}Fe_{0.02}Cl_3$ the 300-cm^{-1} exciton was studied in detail as a function of temperature. The results for the integrated intensity given in Fig. 7 show no distinct inflection point for temperatures below 20 K. Instead, a general decrease in intensity with increasing temperature is seen, with a gradual flattening out occurring between 12 and 20 K. We conclude that the Fe^{2+} ions do disrupt the initial partial 3D magnetic ordering in $CsCoCl_3$, lowering T_N^{I} to ≈ 16 K for $x=0.02$ and blurring the transition temperature. At low temperatures the 300-cm^{-1} exciton should show the effects of any full 3D order ($T<T_N^{\mathrm{II}}$) by resolving into four components, as was found for $CsCoBr_3$ and $RbCoCl_3$.[20,21] The low-temperature spectra, however, show no evidence of this, and the peak frequency and intensity data of Fig. 7 confirm[21] the absence of any fully ordered 3D phase above 3 K. The lowest exciton for the $x=0.06$ crystal was not analyzed in detail because the lowest-temperature spectra provided no evidence of long range 3D magnetic ordering.

The 1D magnon excitations in $CsCoCl_3$ are well described by the effective spin, $S=\frac{1}{2}$, exchange Hamiltonian[4]

$$H_{\mathrm{ex}}=2J_1\sum_i [S_i^z S_{i+1}^z+\epsilon(S_i^x S_{i+1}^x+S_i^y S_{i+1}^y)]\ ,\quad 0<\epsilon<1 \tag{1}$$

where J_1 is the intrachain antiferromagnetic exchange parameter. For temperatures below T_N^{I} the additional structure observed in the magnon scattering at $\mathbf{k}=0$ is adequately described by the effective Hamiltonian[4]

$$H_{\mathrm{eff}}=H_{\mathrm{ex}}+h\sum_i (-1)^i S_i^z\ , \tag{2}$$

where

$$h=h_0+2J_2\sum_\delta \langle S_{i+\delta}^z\rangle\ . \tag{3}$$

Here, h_0 results from the inclusion of single-ion exchange mixing, while J_2 is the molecular-field interchain exchange coupling between atom i and its nearest neighbor δ in the same a-b plane. For $CsCoCl_3$ at $T<T_N^{\mathrm{II}}$, $J_1=49.9$ cm^{-1}, $\epsilon=0.12$, $J_2=1.0$ cm^{-1}, and $h_0=0.65$ cm^{-1}.[4] Estimates for these parameters in $CsCo_{1-x}Fe_xCl_3$ may be obtained from the Raman spectra recorded at temperatures $T\ll T_N^{\mathrm{I}}$ and $T\gg T_N^{\mathrm{I}}$.

The $X(ZX)Y$ spectrum of $CsCo_{0.98}Fe_{0.02}Cl_3$ at 3 K shown in Fig. 5 was curve-resolved to yield peaks at frequencies of 82.6, 85.8, 87.4, 89.3, 94.4, 99.9, 101.2, 105.0, 110.0, and 114.9 cm^{-1}. These frequencies are similar to those found for $CsCoCl_3$ at $T\ll T_N^{\mathrm{I}}$.[3] The shoulder at 82.6 cm^{-1}, and the stronger overlapping lines at 85.8, 87.4, and 89.3 cm^{-1} form the origins for the C, B_2, B_1, and A series[4] of magnetic excitations, respectively, in the $x=0.02$ crystal. The separations between the B_2, B_1, and A lines indicate $J_2=0.9$ cm^{-1}, which is slightly less than that in pure $CsCoCl_3$. The interchain exchange could not be determined from the $x=0.06$ results.

At higher temperatures, $T\gtrsim 2T_N^{\mathrm{I}}$, the upper and lower bounds of the magnon Raman scattering continuum are given to first order in ϵ by $\omega_\pm=2J_1(1\pm 2\epsilon)$.[4] The upper bound is difficult to determine in $CsCo_{1-x}Fe_xCl_3$ because of the overlap with the E_{1g} phonon. There is strong symmetry-allowed coupling between the magnon and this phonon, as will be discussed later. From an analysis of the $x=0$ spectrum at 50 K, the $x=0.02$ spectrum at 40 K, and the $x=0.06$ spectrum at 20 K, we find $J_1\approx 46$ cm^{-1} and $\epsilon\approx 0.13$ independent of the Fe^{2+}-ion concentration. These values for J_1 and ϵ are in general agreement with the neutron scattering results.[4] Thus, within the limitations of the analysis, we conclude that for $x\lesssim 0.06$ the Fe^{2+} ions with their competing anisotropy do not affect the Co^{2+}-Co^{2+} intrachain interaction.

B. Fe^{2+} electronic excitations

The prominent extra features appearing in the 4-K $X(ZZ)Y$ mixed-crystal Raman spectra when compared with $CsCoCl_3$ (see Figs. 1–3) are believed to be associated with electronic transitions between states of the lowest Fe^{2+} cubic-field term, $^5T_{2g}(^5D)$, split by the combined effects of a trigonal distortion to the crystal field, spin-orbit coupling, and a magnetic exchange interaction with adjacent Co^{2+} ions. We shall first consider the $x=0.02$ spectrum, as the new structure is most clearly resolved in this case. Assuming a random doping of Fe^{2+} ions throughout the sample, at the $x=0.02$ doping level there is a 96% probability that a particular Fe^{2+} ion will have two Co^{2+} ions as nearest neighbors along the chain,

with the remaining 4% being predominantly $\cdots$ CoFeFeCo $\cdots$ clusters (Fe^{2+} single ion and Fe^{2+}-Fe^{2+} pairs, respectively, in the nomenclature of Ref. 15). Thus, for $x=0.02$, Fe^{2+} single ions should dominate the dopant scattering.

Johnstone and Dubicki[22] have discussed the ${}^5T_{2g}({}^5D, 3d^6)$ energy levels for a D_{3d} crystal field with spin-orbit coupling, in a study of Raman scattering from $CdI_2(Fe^{2+})$, using an effective Hamiltonian of the form

$$H_{\text{eff}}({}^5T_{2g}, D_{3d})=\Delta[L_Z^2-\tfrac{1}{3}L(L+1)] +\lambda S_Z L_Z+\lambda'(S_X L_X+S_Y L_Y) +\kappa(\mathbf{S}\cdot\mathbf{L})^2+\rho(L_x^2S_x^2+L_y^2S_y^2+L_z^2S_z^2)\ . \tag{4}$$

Here, XYZ refer to cubic axes, xyz refer to trigonal axes, Δ is the effective trigonal field parameter, while λ,λ' and κ,ρ are the first- and second-order spin-orbit—coupling parameters, respectively (see Lockwood *et al.*[23] for a more detailed discussion of these terms). Detailed interaction with ${}^5E({}^5D)$ and higher cubic-field terms of the $3d^6$ configuration is not considered directly in this model. Johnstone *et al.*[15] have followed a similar effective Hamiltonian approach for Co^{2+} ions in $CsMg_{1-x}Co_xCl_3$ and have shown that the parametrization of the problem is equally as good as that obtained using a full $3d^7$-configuration crystal-field calculation. In the present case of $CsCo_{0.98}Fe_{0.02}Cl_3$ it is clear that at 4 K there is still a strong antiferromagnetic ordering of the Co^{2+} ions, so that the total effective Hamiltonian for the Fe^{2+} single ion must include a term to describe an exchange interaction between adjacent Fe^{2+} and Co^{2+} ions. Following earlier treatments of $CoBr_2$,[23] $CsMg_{1-x}Co_xCl_3$,[15] and $CsCoBr_3$,[24] we add a molecular-field exchange Hamiltonian to the H_{eff} of Eq. (4) to give an effective Hamiltonian with exchange of the form

$$H'_{\text{eff}}(Fe^{2+})=H_{\text{eff}}({}^5T_{2g}, D_{3d})-2J_{\text{Fe-Co}}\langle S_Z^{\text{Co}}\rangle S_Z\ , \tag{5a}$$

where $J_{\text{Fe-Co}}$ is the exchange-interaction parameter for Fe^{2+}-Co^{2+} pairs and $\langle S_Z^{\text{Co}}\rangle$ is the expectation value of S_Z for the ground state of a Co^{2+} ion adjacent to an Fe^{2+} ion. As for the Co^{2+} cases, the interchain exchange is considered negligible in comparison to the intrachain term, and the latter is confined to intrachain nearest neighbors.[25] In general, one cannot assume that $\langle S_Z^{\text{Co}}\rangle$ for a Co^{2+}-Fe^{2+} pair will be the same as $\langle S_Z^{\text{Co}}\rangle$ for a full-chain Co^{2+} ion (designated by $\langle S_Z^{\text{Co}}\rangle^{\text{FC}}$ in later discussion) so that, at this stage, we use an effective exchange-interaction parameter defined by

$$J'_{\text{Fe-Co}}\equiv J_{\text{Fe-Co}}\langle S_Z^{\text{Co}}\rangle \tag{5b}$$

in the parametrization of the Fe^{2+} single-ion problem.

To carry out the necessary calculation, we have utilized the matrix elements of $H_{\text{eff}}({}^5T_{2g}, D_{3d})$ for a cubic spin-orbit wave-function basis as given in Ref. 22, with the addition of the matrix elements of S_Z in the same basis to give the full $H'_{\text{eff}}(Fe^{2+})$ matrix of Eqs. (5).

Identification of particular Raman features as Fe^{2+} single-ion transitions is not trivial. In the presence of an exchange field there are 14 possible electronic transitions between the ground state and higher states of the ${}^5T_{2g}$ cubic-field term, and although the energy-level pattern is expected to be similar to that found for $CdI_2(Fe^{2+})$,[22] the effect of the exchange interaction on the level spacings is difficult to predict. The first-order spin-orbit parameters λ and λ' were expected to be of the same order of magnitude (≈ 100 cm^{-1}) as that found for $CdI_2(Fe^{2+})$, while Δ was expected to be somewhat smaller in magnitude than the -462 cm^{-1} found for Co^{2+} ions in $CsCoCl_3$,[15] corresponding to a reduction in trigonal distortion in the vicinity of the smaller Fe^{2+} ion. It quickly became apparent that to obtain any reasonable fit to the prominent 48.5- and 61.0-cm^{-1} peaks, the effective pair exchange $J'_{\text{Fe-Co}}$ had to be in the range 17—20 cm^{-1}, and that the weaker features at 180.0, 234.5, and 281.0 cm^{-1}, together with the strong 225.0- and 274.5-cm^{-1} peaks, formed the next manifold of states ($J'=2$ in the notation of Ref. 22). Finally, the broader 390-, 450-, and 469-cm^{-1} peaks were included as the lowest three states of the $J'=3$ manifold. Similar observations and assignments have been made for $RbFeCl_3$.[26] The result of an iterative least-squares fit to these ten levels, weighted inversely as the uncertainties in their wave numbers in the $x=0.02$ spectrum and allowing all five parameters of Eqs. (5) to vary, is given in Table I. While there is clearly extra scattering in the (500—570)-cm^{-1} region of the spectrum where transitions to the remaining four Fe^{2+} single-ion levels are predicted to lie, the structure is poorly resolved and Co^{2+}-Fe^{2+}—pair scattering is also expected to contribute, so that these single-ion levels could not be included in the least-squares fit. The 3.0-cm^{-1} rms deviation of the weighted fit was considered excellent, and predictions discussed below, which are based on this fit, add support to the correctness of the assignments of Table I.

The predominant effect of increasing the Fe^{2+} concentration to $x=0.06$ appears to be an increased damping of the electronic scattering. Thus the weaker features identi-

TABLE I. Comparison of experimental and calculated energies of Fe^{2+} excitons in $CsCo_{0.98}Fe_{0.02}Cl_3$. All quantities are in cm^{-1}. The root-mean-square (rms) deviation of the weighted fit was 3.0 cm^{-1}.

Exciton frequencies		Energy matrix
Experiment	Calculated	parameters
48.5±0.5	49.2	$\lambda=-86.5$
61.0±0.5	59.2	$\lambda'=-76.6$
180.0±1.0	181.1	$\kappa=0.47$
225.0±0.5	223.0	$\rho=-17.2$
234.5±1.0	242.8	$\Delta=-207.5$
274.5±0.5	273.1	$J'_{\text{Fe-Co}}=18.44$
281.0±1.0	285.0	
390.0±1.0	387.6	
450.0±2.0	459.5	
469.0±2.0	469.8	
	508.4	
	553.3	
	564.4	
	565.5	

fied as Fe^{2+} single-ion scattering in the $x=0.02$ case are not seen as clearly in the $x=0.06$ spectrum. At the higher doping level 88% of the Fe^{2+} ions should still be in the single-ion Co-Fe-Co configuration, while 10.6% should now form Fe^{2+}-Fe^{2+} pairs, but the increased linewidths and consequent poorer resolution of the $x=0.06$ spectrum precludes identification of any specific features as being of Fe^{2+}-pair origin. An analysis of pair energy levels such as that carried out for Co^{2+} pairs in $CsMg_{1-x}Co_xCl_3$ (Ref. 15) is not justified here. It is of interest to note the marked reduction in the strength of the Co^{2+} full-chain features (e.g., 88, 299.5, 851.5, and 1189 cm^{-1}) relative to the Fe^{2+} scattering with increase in Fe^{2+} concentration. This change and the previously noted change to 496.5-nm laser radiation for optimization of the $CsCo_{1-x}Fe_xCl_3$ spectra suggest that we are seeing a resonance enhancement of Fe^{2+} electronic scattering and absorption of Co^{2+} full-chain scattering by the doped crystals. If this is the case, one might expect also to see some enhanced Fe^{2+}-Co^{2+}—pair scattering in the $x=0.02$ spectrum—such a possibility is considered below.

C. Full-chain Co^{2+} excitons

Before analyzing the Fe^{2+}-Co^{2+}—pair scattering in detail, it is necessary to know the actual intrapair exchange $J_{Fe\text{-}Co}$ of Eq. (5a) rather than just the effective exchange $J'_{Fe\text{-}Co}$. This requires knowledge of $\langle S_Z^{Co}\rangle$. As pointed out above, $\langle S_Z^{Co}\rangle^{FC}$ for full-chain (FC) Co^{2+} ions is not strictly appropriate to the Fe^{2+}-Co^{2+}—pair situation, but it should nevertheless be a good first approximation. A refit of the Co^{2+} full-chain spectrum was carried out, using the $CsCo_{0.98}Fe_{0.02}Cl_3$ data, to obtain the $J_{Co\text{-}Co}$ full-chain exchange and an estimate of $\langle S_Z^{Co}\rangle$ needed for the Co^{2+} broken-chain and Fe^{2+}-Co^{2+}—pair analyses. The result of the iterative least-squares fit, using the $^4T_{1g}(^4F, 3d^7)$ equivalent of the effective Hamiltonian crystal field plus exchange model of Eq. (5a), is given in Table II. The Co^{2+} full-chain features from the $x=0.02$ spectrum used in this fit were as identified in $CsCoCl_3$,[15,21] but with slightly different frequencies. The parameters of the revised fit vary on average by less than 3% from the $CsCoCl_3$ calculation of Ref. 15. The revised parameters give $\langle S_Z^{Co}\rangle^{FC}=1.325$, and it should be noted that the J ($=36.2$ cm^{-1}) of Ref. 15, Table 4, corresponds to the product $J_{Co\text{-}Co}\langle S_Z^{Co}\rangle^{FC}$ in our present notation. The relationship between the effective isotropic exchange constant (J_1) of Sec. IV A and the isotropic exchange between true spins ($J_{Co\text{-}Co}$) given in Table II is $J_1\simeq 1.7J_{Co\text{-}Co}$.

Within the experimental uncertainties, the full-chain Co^{2+} features of the $x=0.06$ spectrum do not differ in energy from the $x=0.02$ data, so that the parameters of Table II should also be applicable to the $x=0.06$ spectrum.

TABLE II. Comparison of experimental and calculated energies of Co^{2+} full-chain excitons in $CsCo_{0.98}Fe_{0.02}Cl_3$. All quantities are in cm^{-1}. The rms deviation of the fit was 2.4 cm^{-1}.

Exciton frequencies		Energy matrix
Experiment	Calculated	parameters
88.0±0.5	84.4	$\lambda=270.9$
299.5±0.5	298.9	$\lambda'=192.2$
	314.7	$\kappa=24.1$
516.0±0.5	516.5	$\rho=-80.0$
561.0±0.5	560.5	$\Delta=-467.1$
851.5±0.5	851.9	$J_{Co\text{-}Co}=26.46$
	942.8	
1000.5±0.5	996.5	
1080.5±0.5	1084.6	
1153.5±0.5	1153.3	
	1175.6	

D. Broken-chain Co^{2+} excitons

The mean exchange field experienced by a Co^{2+} ion lying adjacent to a dopant Fe^{2+} ion will not be the same as that experienced by the full-chain Co^{2+} ions considered in the preceding subsection and, in general, the trigonal crystal-field distortions will also differ. These differences can give rise to additional features in the Co^{2+} electronic scattering, as discussed in the earlier treatment of Co^{2+} in $CsMgCl_3$. We restrict our attention here to the Co^{2+} broken-chain arrangements,[15] where the intrachain nearest neighbors are an Fe^{2+} ion and a full-chain Co^{2+} ion. At the $x=0.02$ doping level, 96% of Co^{2+} ions which form part of an Fe^{2+}-Co^{2+} pair are, in fact, in a broken-chain arrangement rather than in a Co^{2+} pair (FeCoCoFe) or Co^{2+} single-ion (FeCoFe) situation. Even for $x=0.06$ less than 12% of Fe^{2+}-Co^{2+} pairs form part of Co^{2+} pair or single-ion arrangements. Also, we do not distinguish between the two possible broken-chain arrangements Co(FeCoCo)Co and Fe(FeCoCo)Co—the difference in $\langle S_Z^{Fe}\rangle$ for the two cases is expected to be negligible and the Co(FeCoCo)Co configuration will in any case dominate at the dopant concentrations studied.

The effective Hamiltonian for the Co^{2+} broken-chain (BC) ion [Co^{2+}(BC)] will be a modification of that used for Co^{2+} full-chain [Co^{2+}(FC)], replacing the full-chain exchange term $-2J_{Co\text{-}Co}\langle S_Z^{Co}\rangle^{FC}S_Z$ by an exchange term of the form

$$-2J'_{BC}S_Z=-(J_{Fe\text{-}Co}\langle S_Z^{Fe}\rangle+J_{Co\text{-}Co}\langle S_Z^{Co}\rangle^{FC})S_Z\ , \quad (6)$$

where J'_{BC} is the averaged effective exchange parameter with contributions from both Fe^{2+}-Co^{2+}(BC) and Co^{2+}(BC)-Co^{2+}(FC) exchange interactions. It was known from the Co^{2+}(FC) calculation that the eigenvalues of $H'_{eff}(Co^{2+})$ are generally much more sensitive to change in the exchange parameter than to change in the trigonal field parameter. Thus, in order to estimate the Co^{2+}(BC) exciton energies we retain the parameters λ, λ', κ, ρ, and Δ of the Co^{2+}(FC) fit (Table II) and calculate the appropriate exchange parameter using Eq. (6). The Fe^{2+} single-ion fit of Table I gave $\langle S_Z^{Fe}\rangle=1.510$ for the Fe^{2+} ground state, while $J_{Co\text{-}Co}$ and $\langle S_Z^{Co}\rangle^{FC}$ are known from the Co^{2+}(FC) fit. The only difficulty arises with $J_{Fe\text{-}Co}$. Using $\langle S_Z^{Co}\rangle^{FC}$ as a first approximation to the actual $\langle S_Z^{Co}\rangle$, and the $J'_{Fe\text{-}Co}$ of the Fe^{2+} single-ion fit, we obtain $J_{Fe\text{-}Co}\simeq 13.91$ cm^{-1}. Diagonalization of the Co^{2+}(BC) ef-

TABLE III. Comparison of estimated, experimental, and best-fit energies of Co^{2+} broken-chain excitons in $CsCo_{0.98}Fe_{0.02}Cl_3$. All quantities are in cm^{-1}. The rms deviation of the best fit to the weighted experimental data was 0.7 cm^{-1}.

Estimated	Experiment	Best fit
	Exciton frequencies	
68.2	70.5±0.5	70.3
291.5	290.0±1.0	290.9
304.3	304.5±1.0	304.6
512.3		515.0
547.8	550.0±2.0	550.7
852.4	852.5±1.0	851.3
925.9		927.5
996.3		1012.7
1067.4		1086.3
1146.4		1162.7
1164.6		1182.4
	Energy matrix parameters	
270.9	λ	270.9
192.2	λ'	192.2
24.1	κ	24.1
−80.0	ρ	−80.0
−467.1	Δ	−489.7
28.11	J'_{BC}	27.71

fective Hamiltonian, using the resulting J'_{BC} from Eq. (6), gave a revised value for $\langle S_Z^{Co}\rangle$ which was, in turn, used to recompute $J_{Fe\text{-}Co}$. This iterative procedure rapidly converged to give self-consistent values of $\langle S_Z^{Co}\rangle = 1.316$ (cf. $\langle S_Z^{Co}\rangle^{FC} = 1.325$) and $J_{Fe\text{-}Co} = 14.00$ cm^{-1}, with the estimated Co^{2+}(BC) exciton energies listed in the first column of Table III.

Inspection of the $x = 0.02$ spectrum revealed weak features very close to five of the predicted Co^{2+}(BC) exciton energies as listed in the second column of Table III. Particularly encouraging is the correspondence with the weak peak at 70.5 cm^{-1} in a region where no further Fe^{2+} structure had been expected. If these five Raman lines are assigned as Co^{2+}(BC) scattering and the parameters Δ and J'_{BC} of the broken-chain effective Hamiltonian are allowed to vary, the least-squares fit of the third column of Table III is obtained. The 5% change in Δ from that for Co^{2+}(FC) is not unreasonable. The modified parameters give $\langle S_Z^{Co}\rangle = 1.271$, implying $J_{Fe\text{-}Co} = 14.5$ cm^{-1}, whereas the modified J'_{BC} gives $J_{Fe\text{-}Co} = 13.5$ cm^{-1}. Considering the approximations of the mean molecular-field model for the exchange, such a discrepancy is not surprising and we take the Fe^{2+}-Co^{2+} exchange-coupling parameter to be $J_{Fe\text{-}Co} = 14.0 \pm 0.5$ cm^{-1}, which is a little more than half that of the Co^{2+} full-chain exchange.

E. Other electronic excitations

So far, various features of the Raman scattering in $CsCo_{1-x}Fe_xCl_3$ have been identified with excitations of single Fe^{2+} ions, full-chain Co^{2+} ions, or broken-chain Co^{2+} ions, in each case including an antiferromagnetic exchange interaction with adjacent ions via a mean molecular-field model. As a result of the strong intrachain exchange, we must also consider the possibility of additional structure arising from double excitations of nearest-neighbor ions. Such scattering has already been reported for cobalt ions in $CsCoBr_3$ and $CsCoCl_3$.[15] For the $CsCo_{1-x}Fe_xCl_3$ case one might expect contributions from the double excitation of three types of pairs: Co^{2+}(FC)-Co^{2+}(FC), Co^{2+}(FC)-Co^{2+}(BC), and Co^{2+}(BC)-Fe^{2+}. However, the observed strength of the Fe^{2+} single-ion scattering in comparison with Co^{2+} scattering implies that Co^{2+}(BC)-Fe^{2+}—pair scattering will dominate any other double-excitation contributions.

Even with this restriction, a detailed analysis of the pair scattering is not straightforward. The zero-order state functions for the Co^{2+}(BC)-Fe^{2+}—pair system will be of the form $|\psi_i^{Co}\rangle|\psi_j^{Fe}\rangle$, where $|\psi_i^{Co}\rangle$ and $|\psi_j^{Fe}\rangle$ refer to Co^{2+}(BC) and Fe^{2+} single-ion states, respectively. This gives 180 pair product states with zero-order energies ranging up to ≈ 1740 cm^{-1}. The real difficulty arises in treating the exchange interaction between ions of the pair, as the ground-state values of $\langle S_Z\rangle$ will not be appropriate for the double-excitation pair states. Although one could treat the intrapair exchange explicitly by including a term of the form $-2JS_Z^{Co}S_Z^{Fe}$ in the pair Hamiltonian, while continuing to employ a molecular-field model for exchange with adjacent ions in the chain, such an approach would be of doubtful practical value. The general lack of well-resolved structure in the measured scattering and the inevitable close spacing of predicted pair levels would preclude any specific assignments.

On the basis of the spectrum of zero-order energies for the pair states, it is reasonable to suppose that most, if not all, of the unidentified extra scattering observed, particularly that in the region above 450 cm^{-1} in $X(ZZ)Y$ polarization (see Figs. 2 and 3), arises from Co^{2+}(BC)-Fe^{2+}—pair excitations. [Additional weak broad peaks at frequencies beyond those shown in Fig. 3 were observed in $X(ZZ)Y$ polarization near 1425, 1470, 1545, 1595, 1710, and 1780 cm^{-1}, with no further peaks visible at higher frequencies up to 2000 cm^{-1}.] In several instances this structure prevents the identification of single-ion features.

F. Phonons and magnon-phonon coupling

The frequencies of phonons observed in the $CsCo_{1-x}Fe_xCl_3$ crystals are summarized in Table IV. The assignments to symmetry species are made on the basis of the polarizations of the lines. The five Raman-active lines expected in pure $CsCoCl_3$ have all been identified and their frequencies are in accord with earlier measurements.[3,15,19] The mixed-crystal phonons are sharp single lines (see Fig. 1) consistent with the one-mode behavior expected for these lines.[14] Apart from the E_{1g} mode, the phonon frequencies vary little with concentration up to $x = 0.06$, in accordance with the small overall shift (~ 5 cm^{-1}) in going from $x = 0$ to $x = 1$ (see Table IV). The E_{1g}-phonon frequency decreases with increasing iron concentration, but then must increase at higher x to reach the $x = 1$ value. This initial decrease is probably as-

TABLE IV. Comparison of peak frequencies in cm^{-1} (± 0.5 cm^{-1}) at 4 K for the Raman-active modes in $CsCo_{1-x}Fe_xCl_3$.

Concentration	Mode symmetry				
x	E_{2g}	E_{1g}[a]	E_{2g}	E_{2g}	A_{1g}
0	55.6	116.0	137.6	187.7	264.2
0.02	55.5	115.0	137.5	187.6	263.9
0.06	55.4	113.8	137.2	187.6	263.6
1[b]	49.5	143.5	132.0	180.5	259.5

[a]Taken from the 20-K spectrum, where the line is clearly visible.
[b]Reference 19.

sociated with the Co^{2+} magnon-phonon coupling, which must eventually vanish at higher Fe^{2+} concentrations.

One remaining puzzle is the polarization properties of the A_{1g} mode. According to the usual selection rules, this mode should only be observed in diagonal polarization, but it is seen much more strongly in YX polarization than in ZZ polarization (see Fig. 1). This effect has been noticed before in other magnetic AMX_3 compounds,[3,14,19,21,24] but does not occur in nonmagnetic $CsMgCl_3$.[14] Breitling *et al.*[19] ascribe this behavior to crystal strain, while Johnstone and Dubicki[24] believe it arises from electron-phonon coupling, which would give rise to antisymmetric phonon scattering in YX polarization. The effect of a degenerate electronic ground state on the Raman scattering by phonons has been considered by Churcher and Stedman,[27] who show that additional terms in the scattering tensor arise under such conditions. Application of their theory to $ACoX_3$ compounds predicts that A_{1g}-phonon scattering can occur in YX polarization.[28] Recent Raman results obtained for isostructural $CsCdBr_3$ also reveal anomalous scattering in YX polarization.[29] As this crystal has an electronic singlet ground state, the Churcher-Stedman explanation does not apply. Thus, at present, there is no conclusive explanation of the strength of the A_{1g} scattering in YX polarization, although it is likely that crystal strain and electronic degeneracy considerations may both be involved.

Strong magnon–E_{1g}-phonon coupling has been observed in several $ACoX_3$ compounds and the previous work on this subject has been reviewed recently.[30] The magnon-phonon coupling in $CsCo_{1-x}Fe_xCl_3$ is evident through the pronounced temperature dependence of the E_{1g}-phonon intensity. This phonon is scarcely visible at low temperatures, but increases rapidly in intensity with increasing temperature for temperatures $T \gtrsim T_N^I$ (see Fig. 5, and Fig. 5 of Ref. 3). With increasing x the phonon becomes more prominent at lower temperatures; otherwise, the general behavior with temperature is the same as for $x=0$. Knowing that the Fe^{2+} ions suppress T_N^I, this is clear evidence that a marked change in the magnon-phonon coupling occurs near T_N^I, allowing the phonon contribution to the scattering to be discerned. The magnon-phonon line shape at higher temperatures was analyzed using the damped-harmonic-oscillator (DHO) model,

$$I(\omega)=[\bar{n}(\omega)+1]S\omega_0^2\gamma^2\omega/[(\omega^2-\omega_0^2)^2+\omega^2\gamma^2]\ , \qquad (7)$$

where S, ω_0, and γ are the oscillator strength, frequency, and damping, respectively, and $\bar{n}(\omega)$ is the Bose population factor at frequency ω. The magnon line shape is well approximated by the DHO model for $T \gg T_N^I$.[21] The results obtained from a least-squares fit to the data are

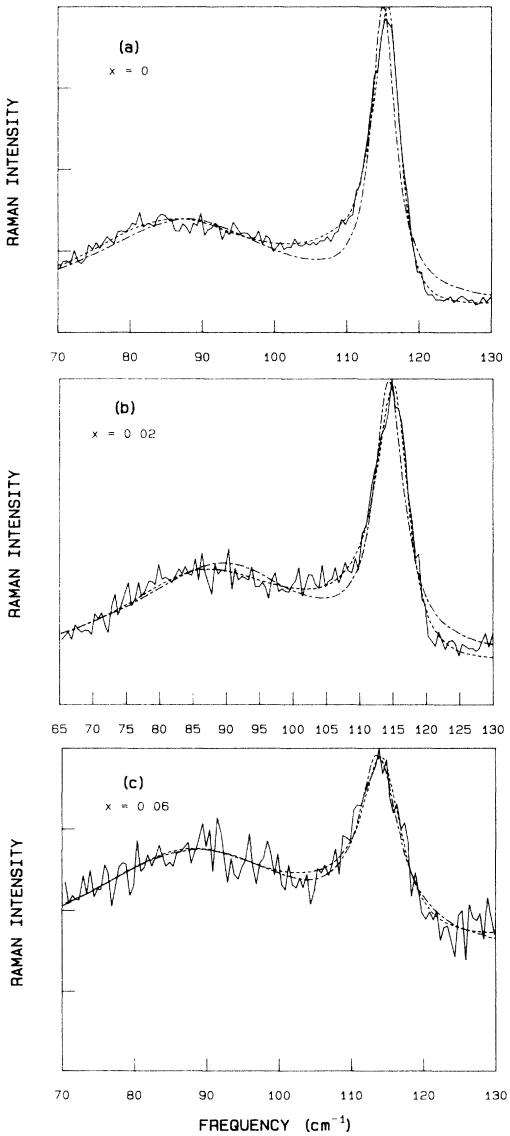

FIG. 8. Results of fits of uncoupled (—·—·—·) and coupled (— — —) harmonic oscillators to the magnon–E_{1g}-phonon Raman spectrum (——) of $CsCo_{1-x}Fe_xCl_3$ for (a) $x=0$ at 50 K, (b) $x=0.02$ at 40 K, and (c) $x=0.06$ at 20 K.

TABLE V. Results obtained from damped-harmonic-oscillator fits to the magnon-phonon spectrum of $CsCo_{1-x}Fe_xCl_3$ and $RbCoCl_3$ in $X(ZX)Y$ polarization. ω_0 denotes the frequency, γ denotes the damping, and c denotes the coupling constant.

		Magnon		E_{1g} phonon		
	Temperature (K)	ω_0 (cm^{-1})	γ (cm^{-1})	ω_0 (cm^{-1})	γ (cm^{-1})	c (cm^{-1})
$CsCo_{1-x}Fe_xCl_3$						
$x=0$	40	91.2	26.7	115.2	4.3	0
		82.7	17.3	119.5	6.4	−18.5
	50	89.2	32.4	115.0	4.0	0
		83.8	27.7	117.3	5.4	−12.4
$x=0.02$	40	90.5	33.0	114.5	5.3	0
		86.5	31.4	116.4	6.6	−9.6
$x=0.06$	20	90.0	38.9	113.7	6.9	0
		87.2	30.4	114.9	7.1	−6.3
$RbCoCl_3$[a]						
	40	97.7	18.5	111.8	4.9	0
		90.3	16.7	114.9	7.0	−13.3
	50	97.5	21.7	111.7	4.7	0
		87.6	19.7	115.1	7.2	−15.7

[a]Reference 21.

shown in Fig. 8, and the parameter values are given in Table V. The DHO model was then modified to include explicitly a symmetry-allowed real coupling[31] between the magnon and E_{1g} phonon. The resultant fits were a significant improvement over the uncoupled model (as can be seen in Fig. 8), particularly for the $x=0$ and 0.02 cases. The coupling constant (see Table V) is concentration dependent, weakly temperature dependent, and comparable with that obtained for $RbCoCl_3$. Despite the approximate nature of the model, several conclusions can be drawn. Doping with Fe^{2+} ions appears to reduce the strength of the magnon-phonon interaction. The magnon peak frequency (and hence J_1) is independent of x, and the E_{1g}-phonon frequency decreases with increasing x, consistent with the earlier peak-frequency analyses. More theoretical work is required to explain the strong spin-phonon coupling in $CsCo_{1-x}Fe_xCl_3$, particularly with regard to the magnon-phonon line shape. Such work is a prerequisite to obtaining more accurate values for J_1 and ϵ.

V. CONCLUSION

This study of magnon and exciton Raman scattering in $CsCo_{1-x}Fe_xCl_3$ has shown that, while the addition of up to 6 at. % of iron has the effect of lowering the 3D magnetic ordering temperature, the 1D intrachain antiferromagnetic ordering characteristic of $CsCoCl_3$ is retained. Analysis of the temperature dependence of the magnon scattering by the Co^{2+} ions in the quasi-1D phase gave an intrachain antiferromagnetic exchange, J_1 (≈ 46 cm^{-1}), and anisotropy, ϵ (≈ 0.13), independent of Fe^{2+}-ion concentration for $x \lesssim 0.06$. Interaction of this magnon with the E_{1g} phonon of $CsCoCl_3$ is, however, significantly reduced by the Fe^{2+} doping, even at the $x=0.02$ level.

Crystal-field analyses of Fe^{2+}, full-chain Co^{2+}, and broken-chain Co^{2+} energy levels, using in each case an effective Hamiltonian appropriate to the respective lowest cubic-field term and a molecular-field model for the antiferromagnetic exchange interaction, give an excellent fit to observed features in the Raman spectrum of the $x=0.02$ crystal. The resulting exchange parameter $J_{\text{Fe-Co}}=14.0$ cm^{-1} for Fe^{2+}-Co^{2+} pairs is somewhat reduced from $J_{\text{Co-Co}}=26.5$ cm^{-1} for the corresponding Co^{2+}-Co^{2+}—pair interaction. Additional scattering present for both $x=0.02$ and 0.06 crystals is believed to be associated with double excitations of Fe^{2+}-Co^{2+} pairs, but the poor resolution of the structure of this scattering has prevented a detailed analysis and assignment to specific pair levels.

For $x \lesssim 0.06$ doping levels the $CsCo_{1-x}Fe_xCl_3$ system has proved to be a particularly interesting and tractable one. While it would also be of interest to follow the effect of higher Fe^{2+} concentration in this system, the damping of the electronic Raman scattering evident in the $x=0.06$ results indicates that there is little likelihood of obtaining good-quality spectra for higher x values. The effect of other paramagnetic dopants such as Ni^{2+}, Mn^{2+}, and Cu^{2+} on the magnetic properties of $CsCoCl_3$ is currently under investigation. Preliminary observations indicate problems in obtaining uniform dopant distribution (for Ni^{2+}), or with an early onset of structural changes (for Mn^{2+} and Cu^{2+}), and it may prove difficult to match the quality of the $CsCo_{1-x}Fe_xCl_3$ data.

ACKNOWLEDGMENTS

We wish to thank R. A. Ritchie (Department of Physics, University of Canterbury) for growing the crystals, B. A. Kettles for computational assistance, and M. R. Miedema (Chemistry Division, National Research Council) for the chemical analyses. One of us (R.W.G.S.) acknowledges the hospitality of the National Research Council of Canada and the Department of Chemistry, University College, London, while on study leave.

---

*Permanent address: Physics Department, University of Canterbury, Christchurch, New Zealand.

[1]N. Achiwa, J. Phys. Soc. Jpn. **27**, 561 (1969).

[2]M. Melamud, H. Pinto, J. Makovsky, and H. Shaked, Phys. Status Solidi B **63**, 699 (1974).

[3]W. P. Lehmann, W. Breitling, and K. Weber, J. Phys. C **14**, 4655 (1981).

[4]S. E. Nagler, W. J. L. Buyers, R. L. Armstrong, and B. Briat, Phys. Rev. B **27**, 1784 (1983), and references therein.

[5]J. P. Boucher, L. P. Regnault, J. Rossat-Mignod, Y. Henry, J. Bouillot, and W. G. Stirling, Phys. Rev. B **31**, 3015 (1985).

[6]P. A. Montano, H. Shechter, E. Cohen, and J. Makovsky, Phys. Rev. B **9**, 1066 (1974).

[7]H. Yoshizawa, W. Kozukue, and K. Hirakawa, J. Phys. Soc. Jpn. **49**, 144 (1980).

[8]M. Steiner, K. Kakurai, W. Knop, B. Dorner, R. Pynn, U. Happek, P. Day, and G. McLeen, Solid State Commun. **38**, 1179 (1981).

[9]W. Knop, M. Steiner, and P. Day, J. Magn. Magn. Mater. **31-34**, 1033 (1983).

[10]H. J. Seifert and K. Klatyk, Z. Anorg. Allgem. Chem. **342**, 1 (1966).

[11]H. Soling, Acta Chem. Scand. **22**, 2793 (1968).

[12]H. F. McMurdie, J. DeGroot, M. Morris, and H. E. Swanson, J. Res. Natl. Bur. Stand. (U.S.) A **73**, 621 (1969).

[13]G. N. Tishchenko, Tr. Kristallogr., Akad. Nauk SSSR **11**, 93 (1955).

[14]I. W. Johnstone, G. D. Jones, and D. J. Lockwood, Solid State Commun. **39**, 395 (1981).

[15]I. W. Johnstone, G. D. Jones, and D. J. Lockwood, J. Phys. C **15**, 2043 (1982).

[16]J. Ferre, J. P. Jamet, J. P. Renard, and B. Briat, J. Phys. C **16**, 1099 (1983).

[17]S. E. Nagler, W. J. L. Buyers, R. L. Armstrong, D. J. Lockwood, and R. A. Ritchie, Physica **120B**, 183 (1983).

[18]N. L. Rowell, D. J. Lockwood, and P. Grant, J. Raman Spectrosc. **10**, 119 (1981).

[19]W. Breitling, W. Lehmann, T. P. Srinivasan and R. Weber, Solid State Commun. **20**, 525 (1976).

[20]D. J. Lockwood and I. W. Johnstone, J. Appl. Phys. **53**, 8169 (1982).

[21]D. J. Lockwood, I. W. Johnstone, H. Labbé and B. Briat, J. Phys. C **16**, 6451 (1983).

[22]I. W. Johnstone and L. Dubicki, J. Phys. C **13**, 121 (1980).

[23]D. J. Lockwood, G. Mischler, I. W. Johnstone, and M. C. Schmidt, J. Phys. C **12**, 1955 (1979).

[24]I. W. Johnstone and L. Dubicki, J. Phys. C **13**, 4531 (1980).

[25]H. Shiba, Prog. Theor. Phys. **64**, 466 (1980).

[26]B. Briat and I. W. Johnstone, in *Raman Spectroscopy,* edited by J. Lascombe and P. V. Huong (Wiley, Chichester, 1982), p. 421.

[27]C. D. Churcher and G. E. Stedman, J. Phys. C **14**, 2237 (1981).

[28]C. D. Churcher, Ph.D. thesis, University of Canterbury, New Zealand, 1981 (unpublished).

[29]C. W. Tomblin, G. D. Jones, and R. W. G. Syme, J. Phys. C **17**, 4345 (1984).

[30]D. J. Lockwood, in *Magnetic Excitations and Fluctuations,* edited by S. W. Lovesey, U. Balucani, F. Borsa, and V. Tognetti (Springer, Berlin, 1984), p. 33.

[31]A. F. Murray and D. J. Lockwood, J. Phys. C **11**, 387 (1978).